





Article

The Impact of Lanthanum and Zeolite Structure on Hydrocarbon Storage

Rasmus Jonsson, Phuoc Hoang Ho , Aiyong Wang , Magnus Skoglundh  and Louise Olsson * 

Competence Centre for Catalysis, Chalmers University of Technology, SE-412 96 Göteborg, Sweden; rasmus.jonsson@chalmers.se (R.J.); phuoc@chalmers.se (P.H.H.); aiyong@chalmers.se (A.W.); skoglundh@chalmers.se (M.S.)

* Correspondence: louise.olsson@chalmers.se; Tel.: +46-31-772-4390

Abstract: Hydrocarbon traps can be used to bridge the temperature gap from the cold start of a vehicle until the exhaust after-treatment catalyst has reached its operating temperature. In this work, we investigate the effect of zeolite structure (ZSM-5, BEA, SSZ-13) and the effect of La addition to H-BEA and H-ZSM-5 on the hydrocarbon storage capacity by temperature-programmed desorption and DRIFT spectroscopy. The results show that the presence of La has a significant effect on the adsorption characteristics of toluene on the BEA-supported La materials. A low loading of La onto zeolite BEA (2% La-BEA) improves not only the toluene adsorption capacity but also the retention of toluene. However, a higher loading of La results in a decrease in the adsorbed amount of toluene, which likely is due to partial blocking of the pore of the support. High loadings of La in BEA result in a contraction of the unit cell of the zeolite as evidenced by XRD. A synergetic effect of having simultaneously different types of hydrocarbons (toluene, propene, and propane) in the feed is found for samples containing ZSM-5, where the desorption temperature of propane increases, and the quantity that desorbed increases by a factor of four. This is found to be due to the interaction between toluene and propane inside the structure of the zeolite.

Keywords: HC trap; cold start; toluene; gasoline; zeolite; lanthanum; La-BEA



Citation: Jonsson, R.; Ho, P.H.; Wang, A.; Skoglundh, M.; Olsson, L. The Impact of Lanthanum and Zeolite Structure on Hydrocarbon Storage. *Catalysts* **2021**, *11*, 635. <https://doi.org/10.3390/catal11050635>

Academic Editors: Maria Casapu and Dmitry E. Doronkin

Received: 31 March 2021

Accepted: 12 May 2021

Published: 15 May 2021

Publisher's Note: MDPI stays neutral with regard to jurisdictional claims in published maps and institutional affiliations.



Copyright: © 2021 by the authors. Licensee MDPI, Basel, Switzerland. This article is an open access article distributed under the terms and conditions of the Creative Commons Attribution (CC BY) license (<https://creativecommons.org/licenses/by/4.0/>).

1. Introduction

Efficient exhaust after-treatment is vital to reduce the emissions of harmful bi-products from combustion engines, such as nitrogen oxides (NO_x), carbon monoxide, unburnt hydrocarbons (HC), and particulates. Modern catalytic converters are efficient in removing these species when operated within the designated temperature range. However, during the warm-up period after a cold-start of the engine, the efficiency of catalytic converters is sharply reduced. Therefore, different trapping materials can be used to delay the unwanted bi-products until the converter has reached operating temperature, i.e., above the so-called light-off temperature. NO_x-adsorbers and HC traps are in this connection interesting techniques [1–4] since 80–90% of all pollutants from vehicles are released during cold starts [3].

The light-off temperature occurs around 300–350 °C for a three-way catalyst (TWC) [5]. Ideally, an HC trap should release the adsorbed hydrocarbons in the light-off temperature range. However, HC traps usually release hydrocarbons around 200–250 °C [5]. Closing this temperature gap is urgent and calls for more research in the field of HC traps. Development of effective adsorbents in terms of high uptake of HC at low temperature, compatible desorption temperatures with the active temperature window for the TWC, and high resistance to hydrothermal aging is crucial [6]. In this regard, zeolites have been widely used for the development of HC traps [5,7]. The temperature range for the desorption of HC from the trapping material depends on the interaction between the hydrocarbons and the zeolite. The characteristics that are highly relevant for this interaction are the pore and channel sizes of the zeolite and its acidity (Brønsted and Lewis acidity) [8–12]. Pore

and channel sizes are dependent on the zeolite type, whereas acidity is strongly regulated by the Si/Al-ratio that affects the Brønsted acidity or by the presence of ion-exchanged cations that induce Lewis acidity [5,8–12].

Toluene is a common HC component in gasoline, however, measurements of the distribution of HC components during cold-start emissions indicate that ethene is the most redundant one, while toluene is the largest component if calculated based on carbon atoms [13]. For this reason, propene (which has properties similar to ethene) and toluene are commonly used to study HC traps [14–16]. These two components interact differently with the zeolite framework. Propene is suggested to adsorb on the OH groups of the Brønsted acid sites by forming hydrogen bonds via the π -electrons in the C=C bond of the propene molecule [17]. Since Brønsted acidity is governed by low Si/Al-ratio, the trapping of propene is enhanced by low Si/Al-ratio. Toluene has been proposed to interact with both Lewis acid sites and Brønsted acid sites [9,18]. Lewis acid sites, such as the negatively charged oxygens in the zeolite framework, have been proposed to interact with the methyl group of the toluene molecule [18,19]. Brønsted acid sites, in contrast, have been proposed to interact with the phenyl ring in toluene [11,18–22].

Lowering the Si/Al-ratio leads to an increased number of Brønsted acid sites, which enhances the adsorption of propene and ethylene in the porous structure of the zeolite. However, this also increases the adsorption of water since the zeolite becomes more hydrophilic. Studies have shown that water competes with smaller HCs for Brønsted acid sites. This is due to the strong interaction between Brønsted acid sites and water, and therefore, water inhibits HC adsorption [23,24]. Ivanov and co-workers have reported that the SiO₂/Al₂O₃-ratio of ZSM-5 does not significantly influence the adsorption of small alkanes (e.g., propane and butane) in the presence of moisture [25]. Increasing the Si/Al-ratio, in contrast to decreasing it, governs the adsorption of toluene in the zeolite. Burke et al. [26] have studied thermal aging of La-BEA and measured the adsorption of toluene and propene using temperature-programmed desorption (TPD). They found a reduction in the adsorption capacity of propene onto La-BEA caused by the dealumination during thermal aging [26]. These findings indicate a connection between the Si/Al-ratio and the Brønsted acidity, which subsequently affects the adsorption patterns in the porous structure of the zeolite.

Zeolites are often ion-exchanged with cations in order to increase the Lewis acidity in HC traps. Ag⁺ has proven to be an efficient addition to HC traps. The positive effects of the silver ion have been attributed to its size and water resistance [5,24,27,28]. The size of an ion-exchanged cation is of major importance for larger molecules to adsorb. For this reason, there have been several studies on Na⁺ in which it acts as a Lewis acid when ion-exchanged in the zeolite [29]. A commonly studied metal for HC storage is Pd [28,30–32]. Lupescu et al. have found that Pd together with Brønsted acid sites promote polymerization of stored HC compounds in the zeolite when gasoline is direct-injected into the exhaust after-treatment system of a Ford Focus passenger car [31].

We have recently studied the effect of impregnating H-BEA with Fe, La, and Pd on the HC-trapping ability of the sample formation [33]. We found that incorporation of La contributed to the adsorption of toluene in zeolite BEA and increased binding strength of the hydrocarbon. However, to our knowledge, no studies have examined the effect of lanthanum loading and the effect of incorporating La into different zeolite structures, which is the objective of the present study. Therefore, we investigate the effect of zeolite structure—ZSM-5 (MFI), Beta (BEA) and SSZ-13 (CHA)—and the effect of La addition to H-BEA and H-ZSM-5 on the storage capacity of toluene, propene, and propane by temperature-programmed desorption (TPD) and diffuse reflectance infrared Fourier transform spectroscopy (DRIFTS).

2. Results and Discussion

2.1. Catalyst Characterization

The catalysts were characterized using N₂ physisorption, Inductively coupled plasma, sector field mass spectrometry (ICP-SFMS), and X-ray diffraction (XRD). The elemental compositions, specific surface area, and total pore volume of the samples are summarized in Table 1.

Table 1. Compositions and textural properties of the catalyst samples.

	BEA	2% La-BEA	6% La-BEA	9% La-BEA	2% La-ZSM-5	ZSM-5	SSZ-13
SiO ₂ /Al ₂ O ₃ ^a	20.2	20.6	21.0	21.4	20.5	20.2	25.2
La wt.% ^a	-	2.2	6.4	8.6	2.0	-	-
La/Al ^a	-	0.14	0.43	0.62	0.12	-	-
S _{BET} (m ² g ⁻¹)	569	467	433	420	330	356	638
S _{micropore} (m ² g ⁻¹) ^b	354	327	305	294	253	273	598
V _p (cm ³ g ⁻¹) ^c	0.65	0.59	0.53	0.52	0.17	0.18	0.34
V _{micropore} (cm ³ g ⁻¹) ^b	0.17	0.16	0.15	0.14	0.12	0.13	0.29

^a Elemental compositions were analyzed with ICP-SFMS; ^b specific surface area and specific micropore volume (S_{micropore} and V_{micropore}) were determined with the t-plot method; ^c total pore volume V_p was calculated at p/p₀ = 0.97.

The N₂ physisorption isotherms for H-SSZ-13 and H-ZSM-5 are close to type I, and the N₂ physisorption isotherm for H-BEA is similar to type IV (IUPAC classification of adsorption isotherms) [34]. The isotherms for all three samples reveal the presence of microporosity with enhanced N₂ uptake at very low relative pressure ranges (Figure A3 in Appendix A). A small hysteresis between the adsorption and desorption isotherms was observed for both H-ZSM-5 and H-SSZ-13, indicating a minor contribution of inter-crystal mesoporosity. The hysteresis was more pronounced for H-BEA. Thus, H-BEA has a lower ratio of micropore volume per total pore volume than H-ZSM-5 and H-SSZ-13 (Table 1). The impregnation with La leads to a decrease of the specific surface area for the BEA and ZSM-5 samples, in line with previous studies [25].

To observe the crystalline state of the samples, X-ray diffraction was used for H-BEA, 2% La-BEA, 2% La-BEA loaded with toluene, 6% La-BEA, 9% La-BEA, H-SSZ-13, and H-ZSM-5 samples. The XRD results are shown in Figure 1. All five BEA samples show the characteristic diffractogram for zeolite BEA [35]. The diffractograms for the ZSM-5 and SSZ-13 samples agree well with reported XRD patterns [36,37]. The samples containing zeolite BEA are compared in Figure 1B. The reflection intensity for the La-doped samples is lower than that for the parent BEA zeolite. This can be due to either a partial collapse of the framework [38] or enhanced X-ray absorption in the presence of La [39]. Moreover, the reflection of 2θ = 22.5° is slightly shifted to higher angles for all La-BEA samples. This reveals that the unit cell of the zeolite is contracted with the incorporation of La. Such contraction of the unit cell has previously been observed for zeolites modified with rare-earth elements [38].

However, the shift is not significantly different for the La-BEA samples with increasing La loadings from 2 to 9% (Figure A1). This suggests that only a certain amount of La can be incorporated in the zeolite, and therefore a further increase of La loading does not contract the unit cell further. Note that although no segregation phase of La₂O₃ has been identified, the oxidation state of 3+ has been reported for La cations in La-doped zeolites [40].

Figure 1C shows the enlargement of the X-ray diffraction pattern for the 2% La-BEA sample saturated with toluene at 80 °C. In contrast to the modification with La, the adsorption of toluene leads to a shift of the main reflection to a lower reflection angle (2θ), indicating an expansion of the unit cell of the zeolite structure due to the confinement of toluene in the pores of the beta zeolite. Expansion of the unit cell of the host zeolite during the adsorption of guest molecules has previously been reported [41–43].

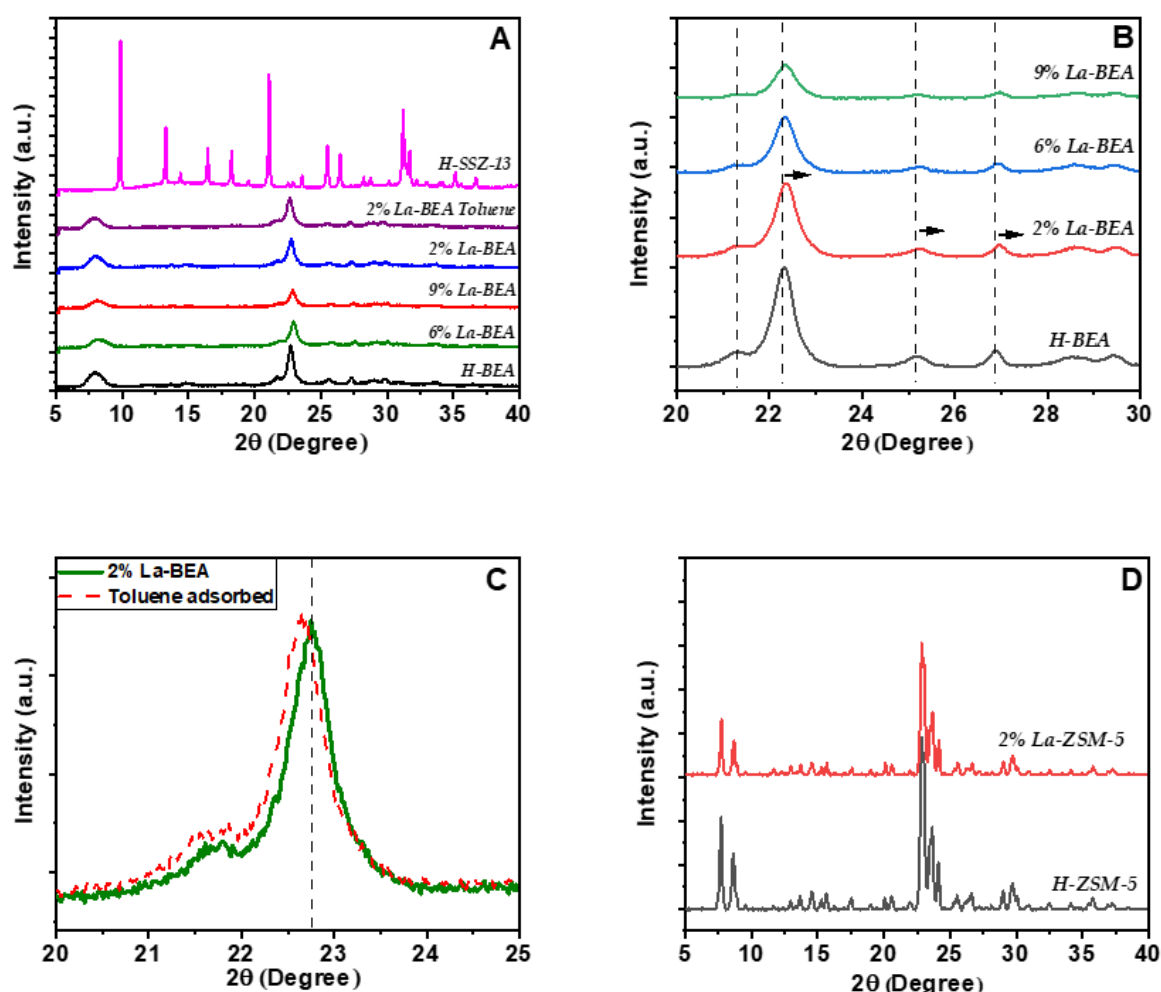


Figure 1. XRD patterns from H-BEA, 2% La-BEA, 6% La-BEA, 9% La-BEA, SSZ-13, ZSM-5, and 2% La-BEA loaded with toluene. Panel (A) series of BEA and HSSZ-13 samples. Panel (B) enlargement of the diffraction patterns for the zeolite BEA samples. Panel (C) comparison of the main reflection of the patterns of the 2% La-BEA and toluene-loaded 2% La-BEA samples. Panel (D) ZSM-5 and 2% La-ZSM-5 samples.

Figure 1D compares the XRD patterns for the ZSM-5 and 2.5% La-ZSM-5 samples. The incorporation of La into ZSM-5 results in a similar characteristic to the La-BEA samples. The intensity of the diffraction peaks for La-ZSM-5 is slightly lower than that for pristine ZSM-5. Moreover, the diffraction peaks for the 2.5% La-ZSM-5 sample are also slightly shifted to higher diffraction angles than those for ZSM-5 due to contraction of the unit cell (Figure A2).

Figure 2 presents the NH_3 -TPD profiles for different adsorbents. Detailed information on the deconvolutions of the profile can be found in Figures A4 and A5 and the amount of desorbed NH_3 and peak desorption temperatures are summarized in Table 2. The desorption profiles for the parent H-BEA and H-ZSM-5 samples show two overlapping peaks at approximately 210–220 °C (low-temperature desorption peak, LTP) and 420–450 °C (high-temperature desorption peak, HTP), corresponding to weak and strong acid sites, respectively [44]. The NH_3 -TPD profile for H-SSZ-13 shows the LTP at 195 °C and the HTP at 458 °C. The amount of acid sites is approximately 599, 755, and 1289 $\mu\text{mol NH}_3/\text{g}$ for H-SSZ-13, H-BEA, and H-ZSM-5, respectively. Both the peak temperature and the total number of acid sites for these parent zeolites are similar to those reported in the literature [45–47]. Impregnation of La leads to a decrease in the intensity of both LTP and HTP for 2%La-ZSM-5 and 2%La-BEA, indicating a decrease in the total number of acid sites (Figure 2). As a result, both 2% La-BEA and 2%La-ZSM-5 show lower total acidity

than the respective parent zeolite (Table 2). For the La-BEA samples, a further increase in La loading also leads to a decrease in total acidity. Deng et al. have reported a similar trend for the incorporation of La into zeolite Y [40]. Our NH_3 -TPD data do not allow us to discuss more the distribution of Brønsted and Lewis acid sites. However, Ivanov et al. [25] found that the addition of 5% La into H-ZSM-5 resulted in a decrease in the number of Brønsted and Lewis acid sites but also in the formation of new sites related to La, e.g., $\text{LaO}(\text{OH})$ and $\text{La}(\text{OH})_2^+$.

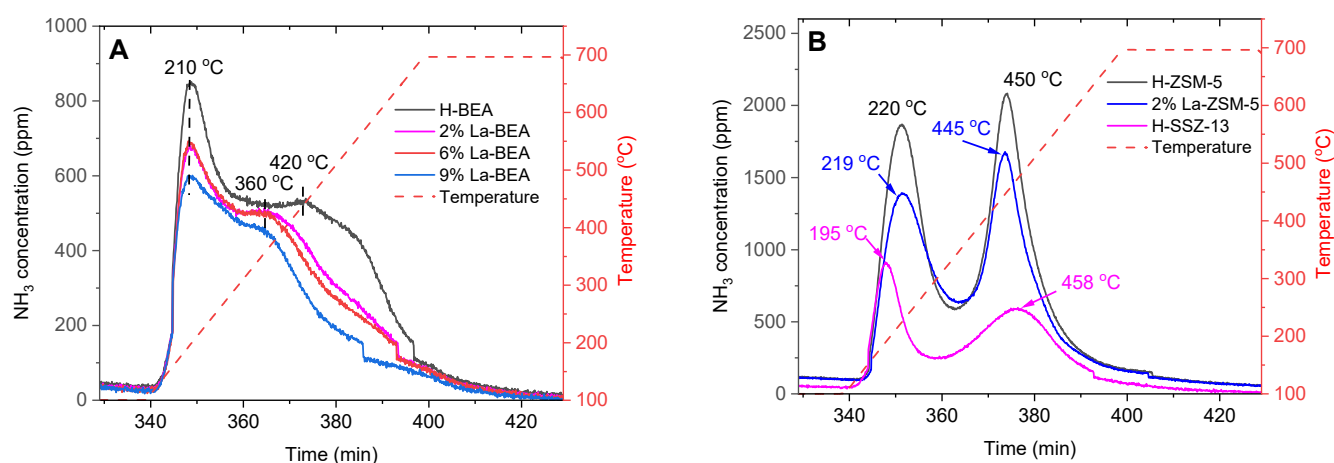


Figure 2. NH_3 -TPD profiles for (A) H-BEA, 2%La-BEA, 6%La-BEA and 9%La-BEA, and (B) H-ZSM-5, 2% La-ZSM-5 and H-SSZ-13.

Table 2. Comparison of acidity for different samples from NH_3 -TPD measurements.

	H-BEA	2% La-BEA	6% La-BEA	9% La-BEA	2% La-ZSM-5	H-ZSM-5	H-SSZ-13
Total acidity ($\mu\text{mol NH}_3/\text{g}$)	755	615	592	506	1093	1289	599
Low-temperature peak (LTP) ($^{\circ}\text{C}$)	213	211	211	210	219	220	195
High-temperature peak (HTP) ($^{\circ}\text{C}$)	420	380	370	348	445	450	458
Percentage of LTP area (%) *	21	19	20	22	43	43	31
Percentage of HTP area (%) *	79	81	80	78	57	57	69

* Detailed information on the deconvolution of the peaks can be found in Figures A4 and A5.

2.2. HC Storage for La-Promoted Zeolites

The goal of an HC-trapping system is to delay the desorption of hydrocarbons released during the warm-up period after a cold-start of the engine in order to oxidize them until the catalytic converter reaches the light-off temperature. One efficient method to measure this is temperature-programmed desorption of hydrocarbons. This study focuses on lanthanum supported on conventional zeolites, such as H-BEA and H-ZSM-5. However, since La is a quite large atom, 3.9 Å in diameter, and the diameter of the eight-membered ring of SSZ-13 is 3.7 Å in diameter, no attempt to impregnate SSZ-13 with La was made. Instead, SSZ-13 was investigated only in the hydrogen form.

Four TPD experiments were performed for eight different samples, and three different types of hydrocarbons were measured. Toluene was chosen since it is a common aromatic in the exhaust during the cold-start period. Further, one alkene and one alkane were used, i.e., propene and propane, to examine the differences when a double bond is present. Each TPD experiment was performed in the presence of 5 vol.% H_2O in the feed since water always is present in real applications of HC trapping. Before each TPD, the samples were pre-oxidized in 10 vol.% O_2 at 400 $^{\circ}\text{C}$ for 20 min and cooled to 80 $^{\circ}\text{C}$ in the presence of H_2O and O_2 . The HC exposure phase was 60 min, followed by flushing the sample in Ar for 20 min, and finally, a temperature ramp was performed at a rate of 20 $^{\circ}\text{C min}^{-1}$. The adsorption of toluene onto the H-BEA zeolite framework has been shown in our previous work to be uninhibited by water due to its low dependency on interaction with Brønsted

acid sites [33]. However, the trapping of propene is strongly affected by the presence of water.

Figure 3A shows the desorption profiles for toluene in the presence of water (wet-toluene TPD) for four samples, i.e., H-BEA and H-BEA promoted with different amounts of La (2, 6, and 9%). Higher desorption quantities were observed for the pure H-BEA and 2% La-BEA samples than for the samples containing higher La loading (6 and 9%). Notably, the 2% La-BEA sample had about a 7% higher storage capacity than the H-BEA sample, which is in line with our previous study [33]. Interestingly, the binding strength of toluene increased when 2% La was incorporated into BEA, resulting in a shift in the desorption maximum temperature of approximately 15 °C. However, when further increasing the amount of La, the adsorption/desorption capacity decreased, as can be seen for the 6% La-BEA and 9% La-BEA samples. It should be noted that of the examined three La loadings, 2% La gave the best results, however, to find an optimum La loading, more concentrations should be examined.

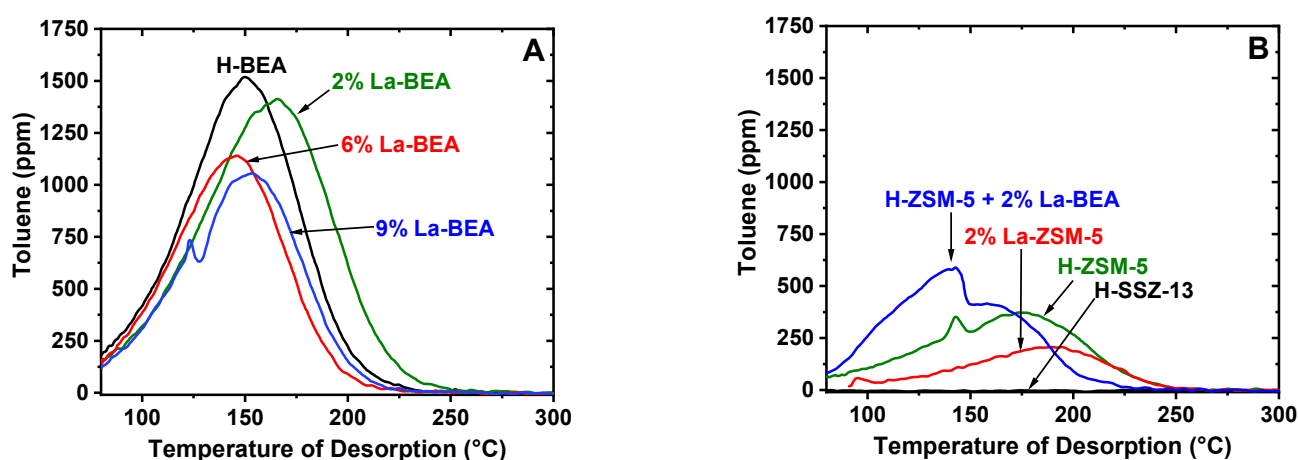


Figure 3. Wet-toluene TPD experiments where toluene desorption is plotted versus the temperature for (A) H-BEA, 2% La-BEA, 6% La-BEA, and 9% La-BEA; and for (B) SSZ-13, ZSM-5, 2% La-BEA, and ZSM-5 + 2% La-BEA.

Figure 3B shows the desorption profiles of toluene for the ZSM-5, SSZ-13, and 2% La-ZSM-5 samples. The profile for SSZ-13 is flat without any toluene desorption, indicating that toluene is not trapped by SSZ-13. This is likely due to the narrow pore size of the zeolite, which may hinder larger molecules, such as toluene, from entering the cages of the zeolite. A lower toluene desorption amount was found for samples containing ZSM-5 compared to BEA samples. Again, the reason is suggested to be the smaller pore size of ZSM-5, which is a medium-pore-sized zeolite with 10-membered rings, compared with BEA, which is a large-pore-sized zeolite with 12-membered rings. However, one advantage with H-ZSM-5 compared to H-BEA is that the binding strength of the toluene is higher, resulting in a shift in the desorption maximum temperature from 150 to 175 °C for the H-ZSM-5 sample compared to the H-BEA sample. Our results for H-ZSM-5 are in good agreement with the study by Serra et al. [48], in which the authors reported a maximum temperature of 175 °C for the desorption of toluene for a sample of H-ZSM-5 with a SiO₂/Al₂O₃-ratio of 20. Moreover, we observed that the toluene storage capacity decreased when the ZSM-5 sample was impregnated with La, which could be suggested to be due to the reduced free-pore volume (as shown in Table 1) resulting in fewer sites for toluene adsorption. This would imply that at a certain loading of La in the zeolite BEA sample, the channels are also partially blocked, which results in a decrease of the pore volume for the adsorption of toluene. A combined sample with a mixture of ZSM-5 and 2% La-BEA was also studied and it gave larger desorption than the H-ZSM-5, but smaller amounts than the 2% La-BEA sample, which is expected.

To summarize, low loadings of La for zeolite BEA have a positive effect on both the amount and the binding strength of toluene. However, a blocking effect was found for

higher loadings (for 6% La-BEA and 9% La-BEA), and the addition of La has a clear effect on the structure of these samples, as found by XRD (Figure 1B).

Figure 4 shows the desorption profiles of propene during wet-propene TPD for the eight samples. Note that a minor amount of propane was also detected during the desorption of propene for some samples, which could be due to minor residues of propane from the cycling experiment before. The results show the only minor formation of propane. In contrast to the corresponding toluene TPD experiment, the BEA zeolite sample exhibited only a small capacity for propene adsorption. This is in agreement with previous studies where BEA samples were examined as HC traps for the adsorption of small hydrocarbons, especially during wet conditions [26,33]. The samples containing ZSM-5 appeared to have the highest storage capacity for propene. Moreover, the H-SSZ-13 sample had a higher temperature of desorption, where the desorption maximum was 137 °C for the H-ZSM-5 sample and 168 °C for the H-SSZ-13 sample. Interestingly, the 2% La-ZSM-5 and the combined samples of 2% La-BEA and H-ZSM-5 performed better than H-ZSM-5 alone. Furthermore, it appears that La also contributes to the adsorption of propene, resulting in a doubled amount of propene desorbed when 2% La was incorporated into ZSM-5. This could be related to the formation of new types of acid sites, $\text{LaO}(\text{OH})$ and $\text{La}(\text{OH})_2^+$.

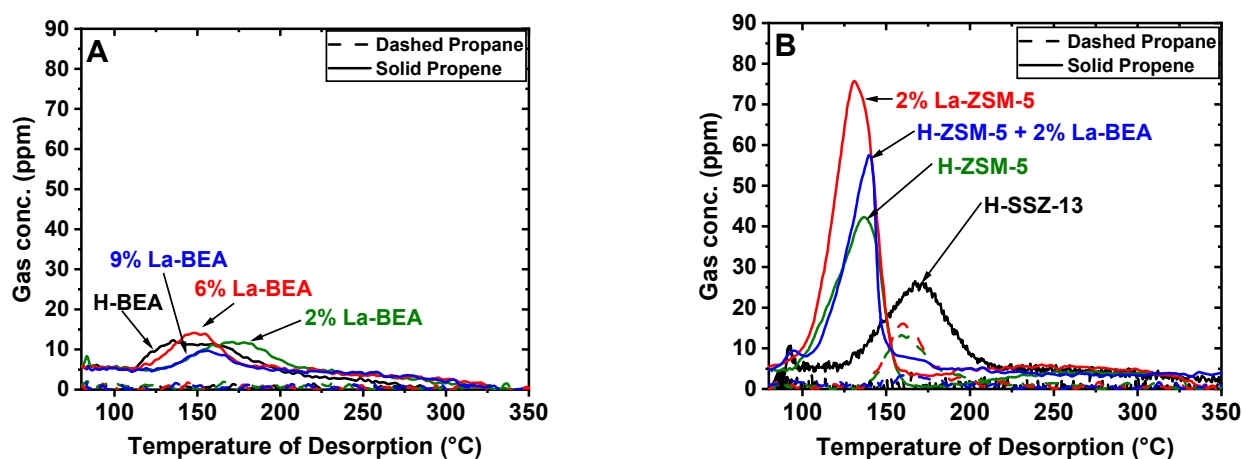


Figure 4. Wet-propene TPD experiments where propene and propane desorption are plotted versus the temperature for (A) H-BEA, 2% La-BEA, 6% La-BEA, and 9% La-BEA; and (B) SSZ-13, ZSM-5, 2% La-BEA, and ZSM-5 + 2% La-BEA.

The desorption profiles of propane during wet-propene TPD are shown in Figure 5. Similar to the propene-TPD profiles, it was found that samples based on zeolite BEA showed a substantially lower amount of propane desorbed than the samples with zeolite H-ZSM-5 and H-SSZ-13. It was observed that the sample containing H-SSZ-13 adsorbed significantly more propane than the other samples and in a quantity similar to the adsorbed propene. The higher propene and propane storage capacity of zeolite SSZ-13 and ZSM-5, which have a smaller pore size than zeolite beta, is likely due to the fact that they hinder the small molecules from desorption compared to large pore beta. For ZSM-5 and the BEA-containing samples, the desorption of propene dominated during the propane TPD, and the profiles of propene desorption are indicated by the dashed lines in Figure 5. A dehydrogenation of propane to propene occurred in the H-SSZ-13 sample but not to the same extent as for the other samples, and propane release dominated (Figure 4B). The conversion of propane into propene in the zeolite BEA and ZSM-5 samples is related to the acidity of the materials. It has been proposed that the Lewis acid sites are beneficial for the dehydrogenation reaction while the Brønsted acid sites are responsible for the cracking reaction of propane in zeolite beta [49]. Note that besides the dehydrogenation reaction, the cracking of propane and the derived product (e.g., propene) could not be discarded. For example, the cracking of propene and dodecane in zeolite BEA during TPD has previously

been reported [32,50]. Westermann et al. [11] have suggested that this process is associated with Brønsted acid sites for zeolite HY with different Si/Al-ratios for hydrocarbon traps.

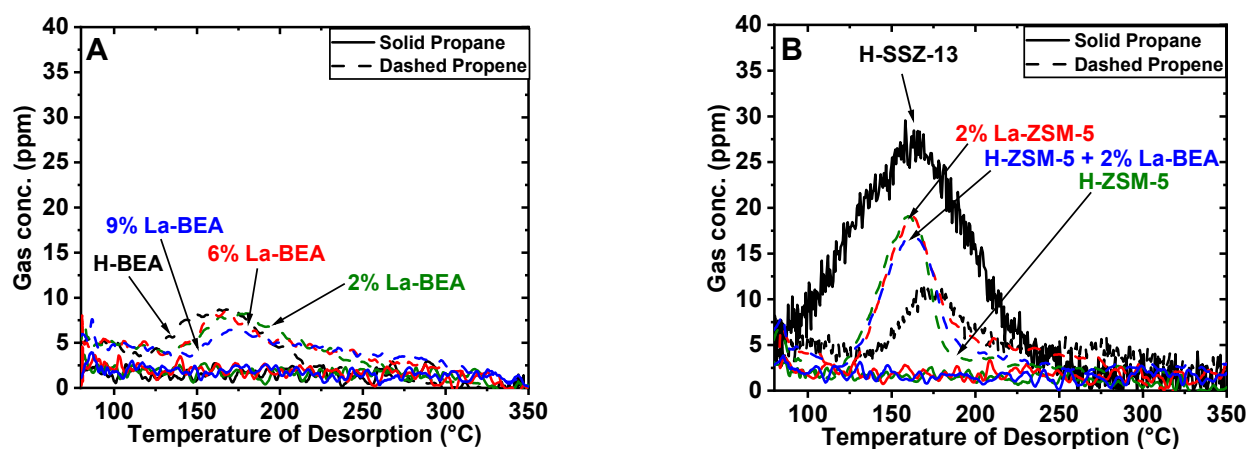


Figure 5. Wet-propane TPD experiments where the desorption of propene and propane is plotted against the temperature for (A) H-BEA, 2% La-BEA, 6% La-BEA, and 9% La-BEA samples; and (B) SSZ-13, ZSM-5, 2% La-BEA, and ZSM-5 + 2.5% La-BEA.

Figure 6 shows a combined wet-HC TPD experiment with toluene, propene, and propane for all eight samples. Panels A and B show the desorption of toluene, and Panels C and D show the desorption of propene and propane, respectively. It can be observed in Figure 6A,B that the desorption profiles and quantities of desorbed toluene are preserved compared to the corresponding desorption profiles for the single toluene TPD experiment (see Figure 2). Azambre et al. have performed mixed HC TPDs that contained a mixture of propene, toluene, and decane [19]. The authors observed competitive adsorption, where over time, larger molecules replaced smaller ones during the exposure phase due to a stronger interaction with the zeolite framework. This may be one explanation for the preservation of the toluene desorption profile found in the present study. Another explanation is suggested to be low competition for storage sites among toluene and the other two HC components, which would result in a preserved toluene desorption profile.

Figure 6B,D shows some changes in the samples containing ZSM-5. The desorbed amount of propene is higher compared to that for propane. Interestingly, the presence of toluene and propene in the feed during the exposure phase resulted in a significant increase in adsorption and desorption of propane. A possible explanation for this can be that propane is hydrophobic, and with the confinement of toluene in the zeolite structure, the number of possible sites for propane to interact with increases. This effect was found to be strongest for the mixed ZSM-5 + 2% La-BEA samples. This might be related to selective adsorption capacity of each material in the mixture, for example, zeolite BEA is more selective towards toluene adsorption while zeolite ZSM-5 prefers to store smaller HC components. Both propane and propene desorbed for the H-SSZ-13 sample in an even distribution, although the quantity was lower than for the corresponding propane TPD and propene TPD experiments. This finding suggests that propene and propane in the H-SSZ-13 sample compete for storage sites, likely due to steric hindrance in the small pores.

The results from the four HC TPD experiments shown in Figures 3–6 have been integrated and presented as bars in Figure 7. H-BEA, 2% La-BEA, 6% La-BEA, and 9% La-BEA samples are shown in Panels A, C, and E, and the remaining samples are shown in Panels B, D, and F. The desorption of toluene was unaffected by the presence of propene and propane, which is clearly seen in the quantified desorption data (Figure 7). As seen in Figure 7A,B, the samples with BEA stored toluene better than ZSM-5, with an increase of about two times, and SSZ-13 was found to have a negligible storage ability. Figure 7F shows that the desorption of propane was enhanced by the presence of toluene, especially for the samples containing ZSM-5. For example, propane desorption increased by as much as four times for the H-ZSM-5 sample when propene and toluene were included during

the adsorption phase, which agrees well with the study by Czaplewski et al. [51]. Even though there was a decrease in propene adsorption/desorption for the complete HC mix for most of the samples (Figure 7D), this is not sufficient to explain the increase in the desorption of propane shown in Figure 7F. Thus, it is clear that the presence of toluene results in enhanced total amount of HC trapped. Moreover, Westermann et al. [11] studied the effect of the presence of three components (propene, toluene, and decane) during HC TPD and compared the capacities of different zeolites in dry conditions. They found that the adsorption capacity of toluene at saturation for zeolite BEA was around 0.2 mmol per gram catalyst, which agrees well with our results in Figure 7A.

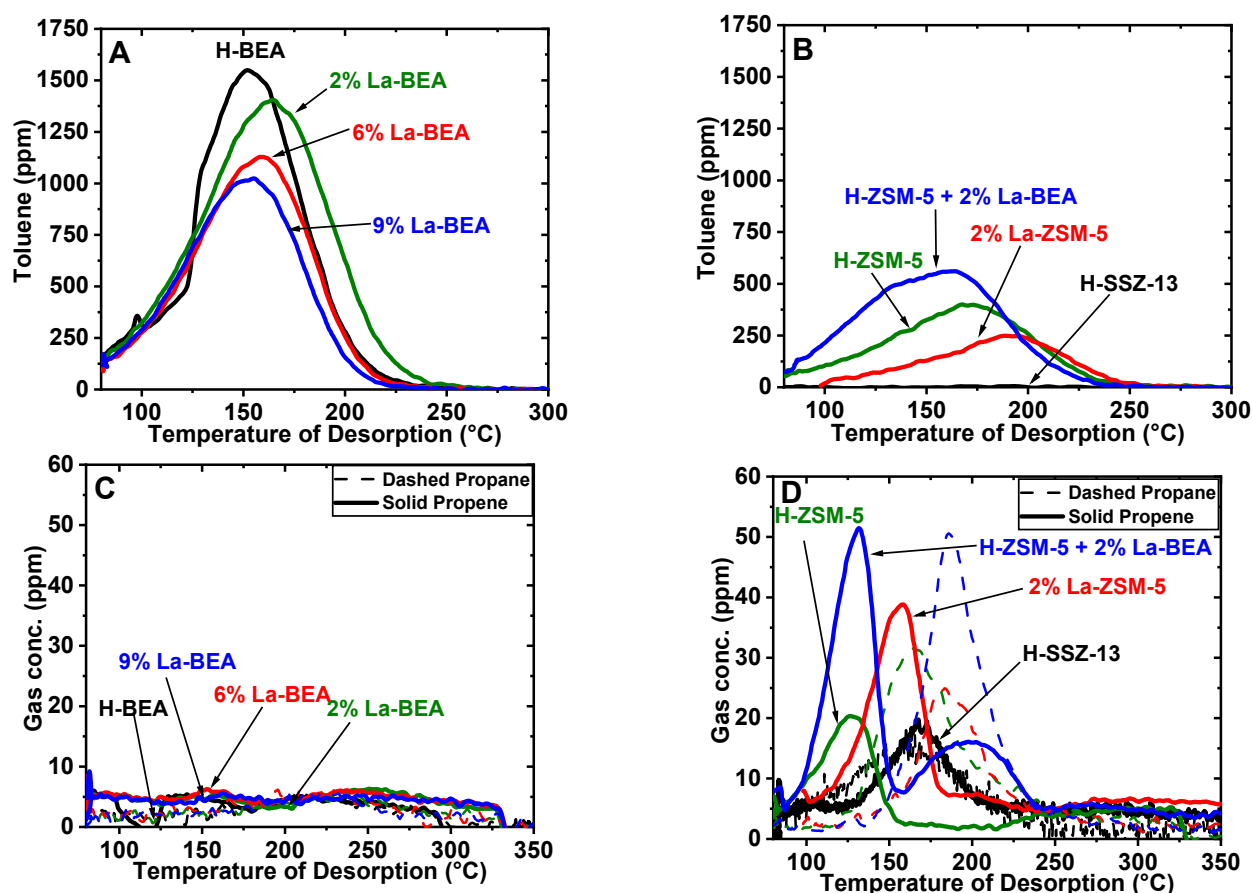


Figure 6. Combined HC TPD experiments where toluene (A,B), and propene and propane (C,D) desorption are plotted versus temperature for (A,C) H-BEA, 2% La-BEA, 6% La-BEA, and 9% La-BEA, and for (B,D) SSZ-13, ZSM-5, 2% La-BEA, and ZSM-5 + 2% La-BEA.

In-situ DRIFTS was used to measure the surface species during toluene TPD. Prior to the TPD experiment, all samples were pre-oxidized at 400 °C with 10 vol.% O₂ for 20 min and cooled to 80 °C in the presence of O₂. This was followed by a dry-toluene exposure phase at 80 °C for 60 min and then cooling to room temperature. The reason for dry-toluene exposure instead of wet was due to the findings in the previous study where the adsorption of toluene was unaffected by water during adsorption and desorption. The toluene exposure step was performed in the same flow reactor as for the HC-TPDs shown in Figures 3–6. Thereafter, the temperature was decreased, and coating with the adsorbents was scraped off from the monolith substrates and studied by in-situ DRIFTS. Two TPDs were performed in the DRIFTS cell. First, a toluene TPD was conducted, where the changes in surface species were measured at different temperatures, thereafter, the samples were oxidized in 10 vol.% O₂ for 30 min at 400 °C in and then cooled to 80 °C in presence of O₂.

After oxidation, a second TPD was performed, which was later subtracted from the first one to remove background signals.

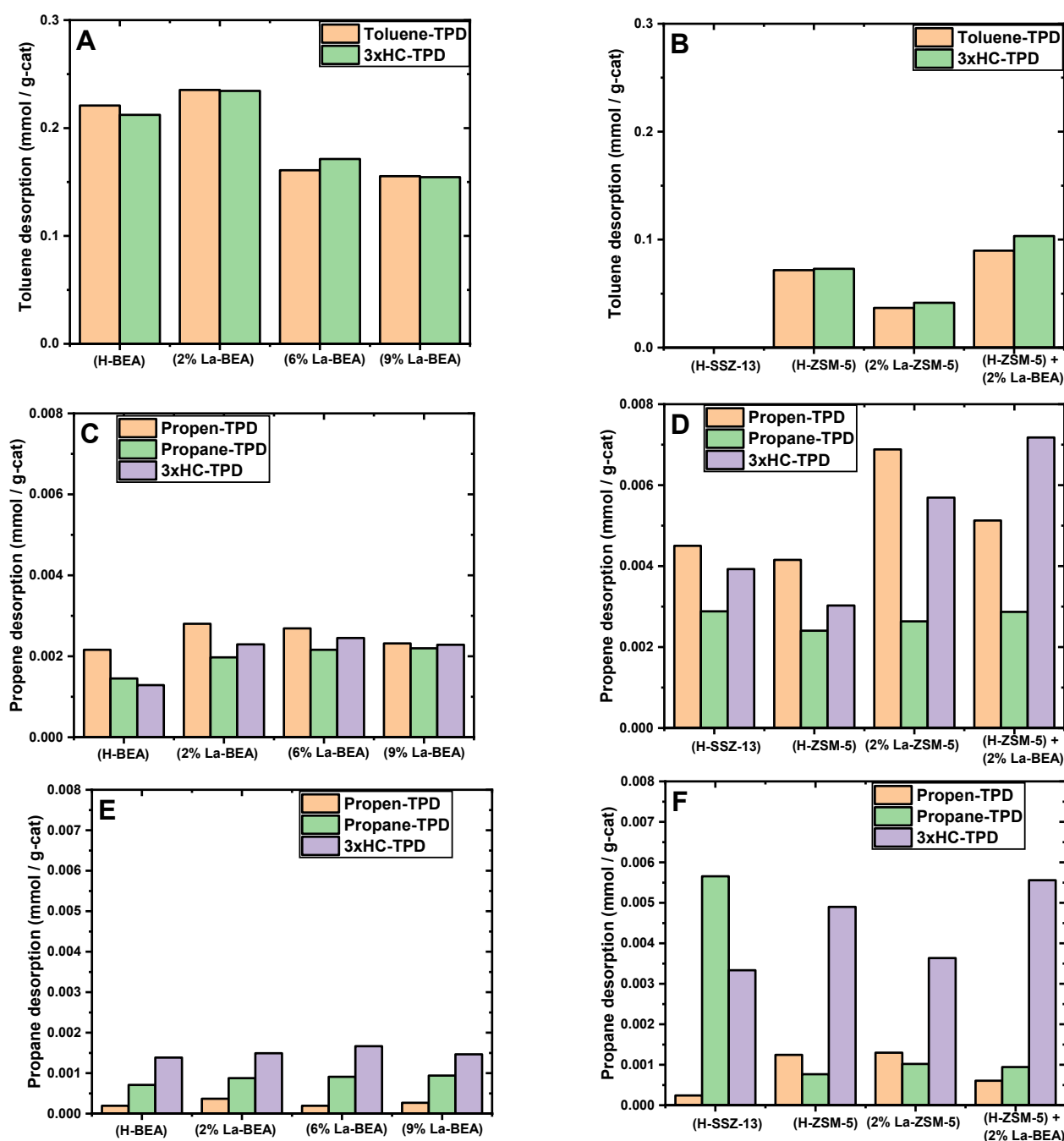


Figure 7. Integrated results from Figures 2–5 where each bar represents the desorbed quantity from each TPD experiment. Panels (A,B) are a quantification of desorbed toluene; panels (C,D) are a quantification of desorbed propene; and panels (E,F) are a quantification of desorbed propane.

The results from in-situ DRIFTS experiments are shown in Figures 8 and 9. Five peaks in the high wavenumber range are strongly associated with adsorbed toluene. The three bands at 3090, 3063, and 3030 cm^{-1} are assigned to the stretching vibrations of the C-H bond of the phenyl-group while the two bands at 2925 and 2873 cm^{-1} are assigned to the asymmetric and symmetric stretching vibrations of the methyl group, respectively [52,53]. As the temperature increased, negative peaks started to grow due to desorption, and it was observed that the negative peaks of samples with a high La loading increased faster than

those for the H-BEA and 2% La-BEA samples, meaning that toluene desorbed faster from the high-loaded BEA samples. A broad peak around 3600 cm^{-1} was observed in the spectra of all samples at $80\text{ }^{\circ}\text{C}$ (Figures 8A and 9A), which possibly can be assigned to hydrogen bonds of adsorbed water [54] because the samples were exposed to air during the transfer from the flow reactor to the DRIFTS cell. The adsorbed water desorbed from the samples when the temperature was increased, and as a result, this broad peak disappeared from the spectra at 150 , 250 , and $350\text{ }^{\circ}\text{C}$ (Figure 8C,E,G and Figure 9C,E,G). There were four peaks at the end of the high wavenumber range, 3780 , 3736 , 3664 , and 3616 cm^{-1} . The band around 3780 cm^{-1} is attributed to the very high frequency (VHF) band, which has been reported for H-BEA and delaminated ZSM-5. The peaks at 3780 and 3664 cm^{-1} are generally assigned to AlOH groups, namely extraframework or partially hydrolyzed alumina species [55,56]. The peak at 3736 cm^{-1} is attributed to terminal silanols while the peak at 3616 cm^{-1} is assigned to Brønsted acid sites (Si-O-Al(O-H)-O-Si) of the zeolites [56–58].

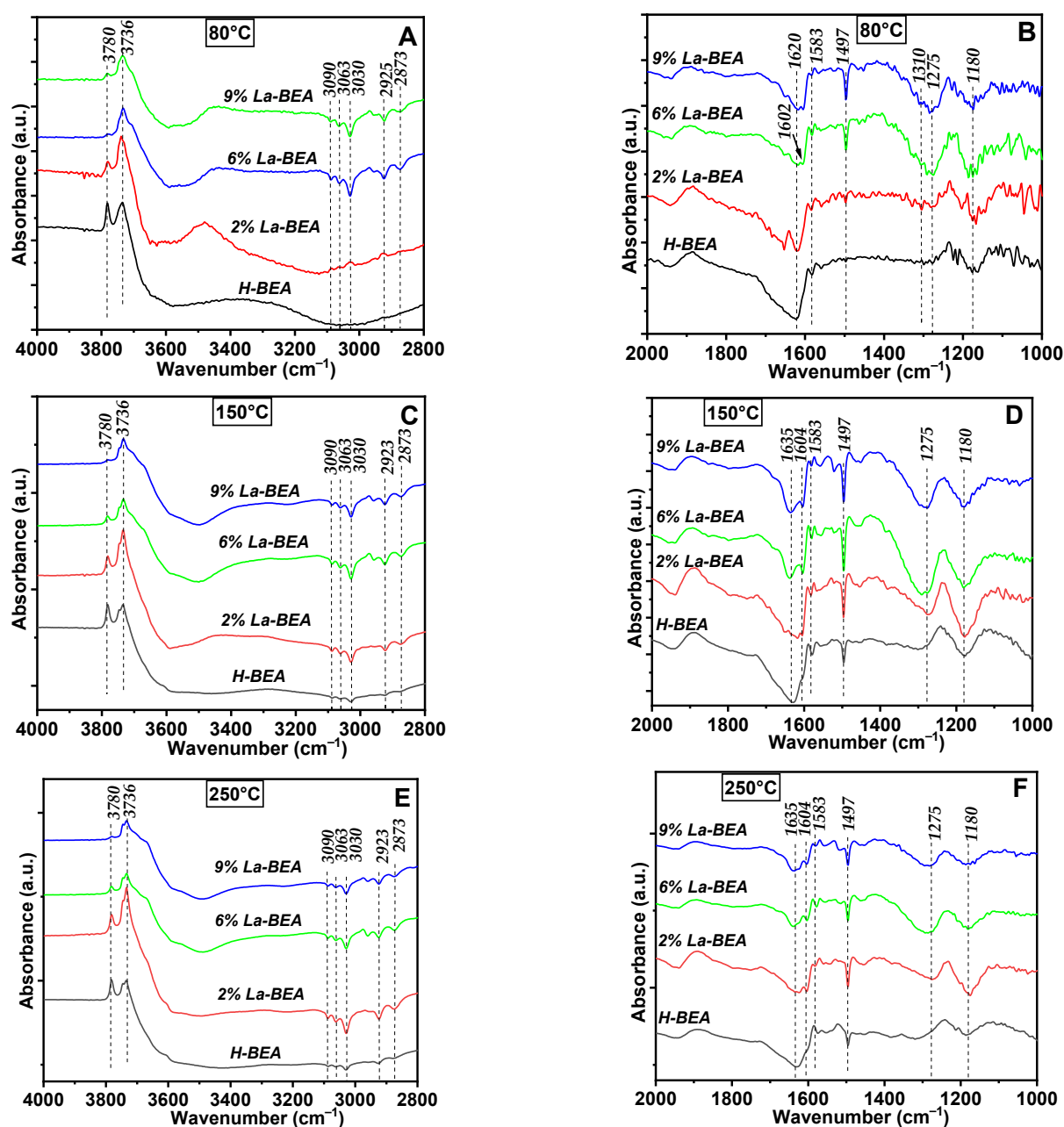


Figure 8. Cont.

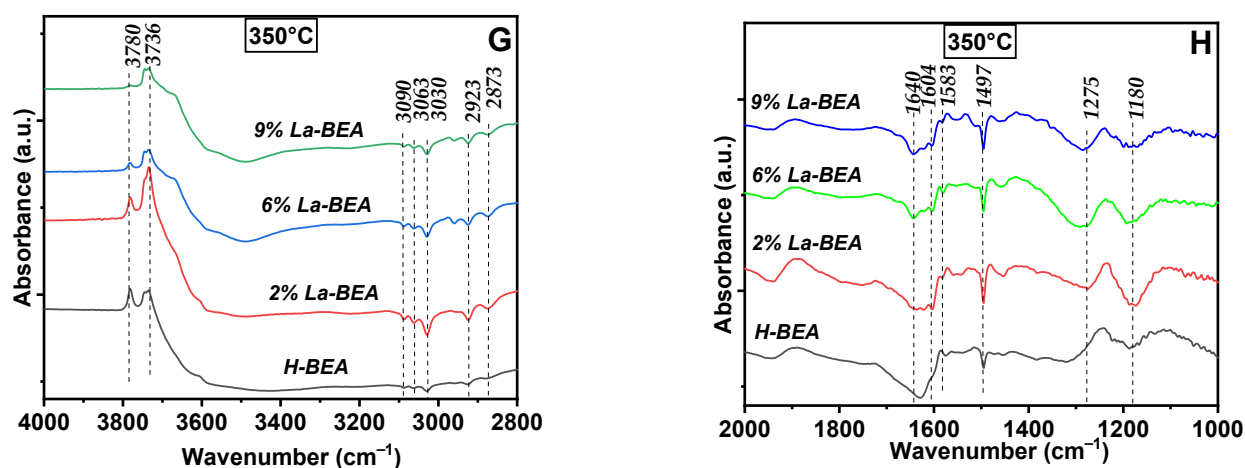


Figure 8. DRIFTS spectra during dry-toluene TPD experiments for H-BEA, 2%La-BEA, 6%La-BEA, and 9%La-BEA. The DRIFT spectra were recorded isothermally at different temperatures in Ar: (A,B) 80°C, (C,D) 150°C, (E,F) 250 °C and (G,H) 350 °C.

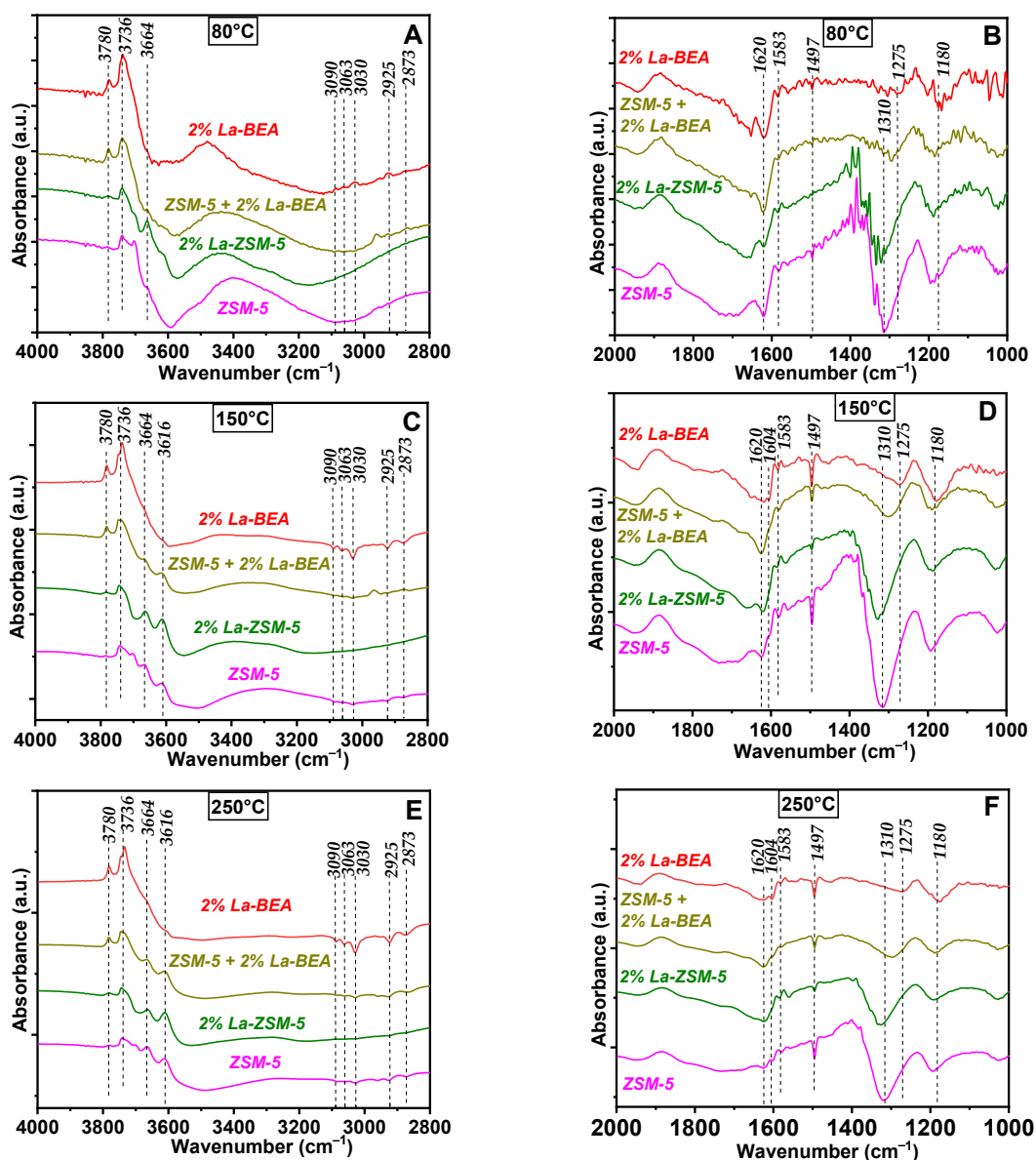


Figure 9. Cont.

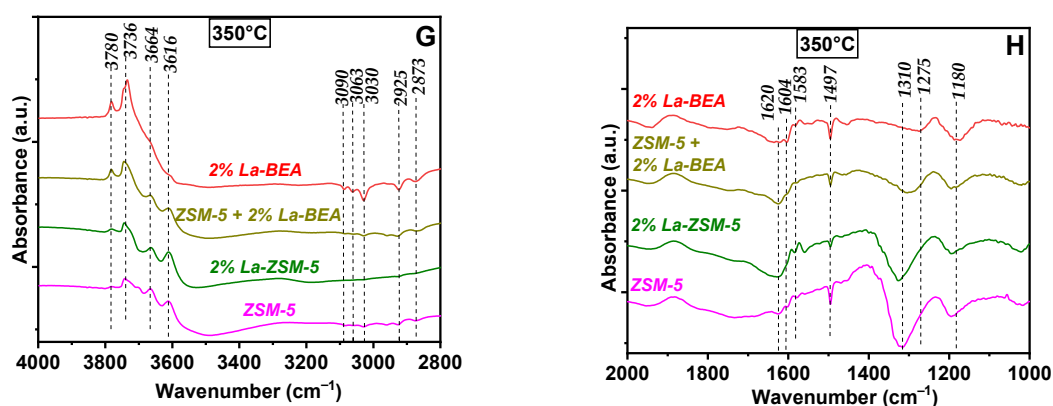


Figure 9. DRIFTS spectra during dry-toluene TPD experiments for H-ZSM-5, 2%La-ZSM-5, 2%La-BEA, and a mixture of 2%La-ZSM-5 and 2%-BEA. The DRIFT spectra were recorded isothermally at different temperatures in Ar: (A,B) 80 °C, (C,D) 150 °C, (E,F) 250 °C and (G,H) 350 °C.

Three peaks at 1602, 1497, and 1275 cm^{-1} in the low wavenumber region are strongly associated with toluene. The peaks 1602 and 1497 cm^{-1} are assigned to the in-plane skeletal vibration of the phenyl group, and the peak at 1275 cm^{-1} is assigned to the symmetric vibrations of C-C [54,59,60]. Peaks at 1602 and 1497 cm^{-1} could be observed for all samples with the ability to adsorb toluene. A peak at 1275 cm^{-1} was found for samples containing BEA. The samples containing ZSM-5 did not have a peak similar to the peak for the BEA samples in this region but at a higher wavenumber. It is reasonable to assume that this peak, located at 1310 cm^{-1} , is also related to the symmetric vibrations of C-C. The peaks occurring around 1620–1640 cm^{-1} are assumed to be associated with the desorption of water on the surface of the zeolite [52,54]. Samples containing La or ZSM-5 showed a dual peak at around 1583 cm^{-1} . In a comparison of toluene-TPD for H-ZSM-5 and Ag-ZSM-5, Liu et al. observed a peak in this region due to the incorporation of silver ions into the pores of ZSM-5, which was assigned to Ag^+ -phenyl [24]. This extra peak was also observed in our previous study, where a similar experiment was conducted with various HC-trap materials (La-BEA included) [33].

Figure A6 shows that no characteristic toluene-related peaks are visible for the H-SSZ-13 sample at 80 °C. The result is consistent with the results for the TPD experiments shown in Figure 3, with no adsorption/desorption of toluene for the H-SSZ-13 sample. This is related to the small pore size for H-SSZ-13, which sterically hinders the adsorption of larger molecules. Figure 8B shows that toluene desorbed from the 6% La-BEA and 9% La-BEA samples at low temperatures, as indicated by the growth of the negative desorption peaks located at 1497 and 1275 cm^{-1} . These results are consistent with the TPD data (Figure 3), in which the desorption of toluene was shifted towards higher temperatures for the 2% La-BEA sample compared to the 6% La-BEA and 9% La-BEA samples. In the high-loaded samples, La might block the access of HC to zeolite pores. Additionally, La can provide new acid sites such as $\text{LaO}(\text{OH})$ and $\text{La}(\text{OH})_2^+$, improving the interaction with toluene. These factors could be reasons for the increased toluene adsorption capacity of the 2% La-BEA sample.

3. Materials and Methods

3.1. Sample Preparation

Three different zeolites were used in the present study: ZSM-5 (CBV2314, theoretical $\text{SiO}_2/\text{Al}_2\text{O}_3$ -molar ratio of 23, NH_4^+ -form), BEA (CP814E, theoretical $\text{SiO}_2/\text{Al}_2\text{O}_3$ -molar ratio of 25, NH_4^+ -form), and SSZ-13 (theoretical $\text{SiO}_2/\text{Al}_2\text{O}_3$ -molar ratio of 25, H^+ -form). Zeolite ZSM-5 and BEA were purchased from Zeolyst International (Conshohocken, Pennsylvania, United States), and SSZ-13 was synthesized using a procedure reported in our previous work [61]. All supports in a form of fine powder were calcined at 550 °C for 2 h to transform from NH_4^+ - to H^+ -form. Four samples with different weight loadings of La,

namely 2.5% La-ZSM-5, 2% La-BEA, 6% La-BEA, and 9% La-BEA were prepared using incipient wetness impregnation. A solution containing a given amount of the precursor $\text{La}(\text{NO}_3)_3 \cdot 7\text{H}_2\text{O}$ was thoroughly mixed with the support material. The mixture was then dried at 120 °C for 24 h followed by calcination at 550 °C for 2 h with a heating rate of 5 °C min⁻¹. One sample consisted of a physical mixture of the 2% La-BEA sample and the H-ZSM-5 zeolite in an equal weight ratio. Zeolite H-SSZ-13 was used without La doping.

The powder samples were then coated onto honeycomb-shaped cordierite monolith substrates (400 cpsi, diameter of 21 mm and length of 20 mm) using a dip-coating procedure with Boehmite (Sasol Dispersal P2, Sandton, South Africa) as a binder. Detailed information on the coating procedure can be found elsewhere [33].

3.2. Material Characterization

The elemental composition of all materials was measured using Inductively Coupled Plasma Sector Field Mass Spectrometry (ICP-SFMS), which was performed by ALS Scandinavia AB.

X-ray diffraction measurements were performed using a Siemens D5000 diffractometer (Siemens, Aubrey, TX, USA) operating at 40 kV and 40 mA. The diffractograms were collected at 2 θ -intervals of 10–80° with a 2 θ -increase of 0.03° per second.

N₂ physisorption measurements were performed using a TriStar 3000 gas adsorption analyzer (Micromeritics, Norcross, GA, USA). Prior to each measurement, approximately 0.1 g of powder sample was degassed at 250 °C for 16 h. The specific surface areas were calculated from the Brunauer–Emmett–Teller (BET) method while the microporous surface area and micropore volume were determined using the t-plot method. The total pore volume was calculated at the relative pressure point of $p/p_0 = 0.97$.

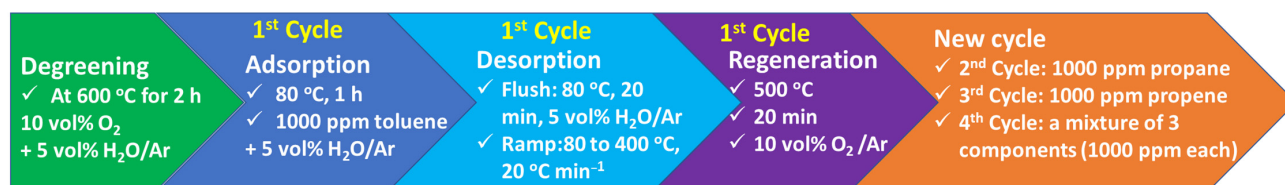
NH₃-TPD measurements were performed using a calorimeter (Sensys DSC, SETARAM instrument, Cranbury, NJ, USA). Powder samples were pelletized and sieved to collect a fraction of particle sizes from 180 to 250 μm . Prior to each analysis, approximately 30 mg of material was pretreated at 300 °C for 30 min in Ar and then cooled to 100 °C. After that, a flow of 20 mL min⁻¹ containing 2000 ppm NH₃ balanced in Ar was introduced into the reactor for 90 min. This duration was sufficient to saturate the sample with NH₃. The sample was then flushed with Ar for 60 min to remove physisorbed NH₃. Temperature-programmed desorption measurements were performed by increasing the temperature from 100 to 700 °C (heating rate 10 °C min⁻¹). The mass number, $m/z = 17$, was recorded to follow the desorption of NH₃ using a mass spectrometer (HPR-20 QIC, Hidden analytical, Warrington, UK).

3.3. Adsorption and Desorption of Hydrocarbons

The coated monolith sample (diameter of 21 mm and length of 20 mm) was wrapped in a thin layer of quartz wool (less than 1 mm) and placed inside a quartz tube (22 mm in diameter and 750 mm in length). Two thermocouples were inserted into the monolith; one in the middle of the monolith to measure the temperature of the sample, and another measured the reactor temperature at approximately 20 mm in front of the monolith sample. The reactor was surrounded by a heating coil, which was subsequently covered with a layer of insulation. Dosage and volumetric flow of gases were controlled using mass flow controllers and a controlled evaporator mixing (CEM) system provided by Bronkhorst (Bethlehem, PA, USA). Gas compositions were analyzed using an MKS Multigas 2030 FTIR spectrometer (MKS Instruments, Andover, MA, USA).

The adsorption and TPD experiments for each sample were performed in four sequential cycles including three cycles with a single gas component (toluene, propane, and propene) and a mixture of those three gases. Each cycle includes an exposure step and a subsequent desorption step. An overview of the tests is shown in Scheme 1. The sample was firstly degreened in 10 vol.% O₂ and 5 vol.% H₂O at 600 °C for 2 h and then cooled to 80 °C in 10 vol.% O₂. The sample was then exposed to a gas flow of 1200 mL min⁻¹ containing 1000 ppm toluene and 5 vol.% H₂O/Ar during the adsorption step of the first

cycle. After that, the sample was flushed for 20 min in a flow of 600 mL min⁻¹ containing 5 vol.% H₂O/Ar. The desorption step was performed by heating the sample from 80 to 400 °C with a rate of 20 °C min⁻¹ in the same flow as the flushing step. A low flow rate in the desorption step was selected to facilitate the analysis of the hydrocarbons with low concentrations.



Scheme 1. Overview of experimental design of sequential tests for each sample. Note that all cycles (cycles 1–4) were conducted in the presence of 5 vol% H₂O.

3.4. In-Situ DRIFTS (Diffuse Reflectance in Farred Fourier Transform Spectroscopy)

To evaluate the interaction of toluene and the zeolite samples, DRIFTS measurements were performed using a VERTEX 70 spectrometer (Bruker, Billerica, MA, USA) equipped with a liquid-nitrogen-cooled mercury cadmium telluride detector, a Praying Mantis™ diffuse reflectance accessory, and a stainless-steel reaction chamber (Harrick Scientific Products Inc., Pleasantville, NY, USA). Spectra were measured between 4000–500 cm⁻¹ with a resolution of 4 cm⁻¹. The second fresh monolith of each sample was loaded in the flow reactor and the degreening and exposure step of toluene were performed with the same as the first cycle described in Section 3.3 but without water. This selection was to simplify the experiment because it had been observed that water did not affect the adsorption of toluene. After that, the powder of the washcoat was removed from the monolith and used for in-situ DRIFT experiments. The powder sample was loaded into a cell and a flow of Ar (100 mL min⁻¹) was introduced. The temperature of the cell was initially set up at 80 °C and increased stepwise to 150, 200, 250, 300, and 350 °C. Data on the desorbed surface species were collected during the temperature steps. After that, the sample was oxidized at 400 °C in 10 vol.% O₂ for 20 min to remove any residual hydrocarbons, and subsequently, cooled to 80 °C in Ar. The second stepwise temperature increase was performed with the same procedure described for data collection so that the background at each respective temperature of the measurements (80, 150, 200, 250, 300, and 350 °C) was recorded.

4. Conclusions

In the present work, we studied the effects of La and zeolite structure on hydrocarbon storage and desorption for HC traps. Adsorption and desorption of both single and multiple HC components were performed by the TPD experiments. The desorption characteristics of toluene during the desorption were also investigated using in-situ DRIFTS. The zeolites used were BEA, ZSM-5, and SSZ-13. The 2% La-BEA sample exhibited a 7% increase in toluene storage/release and 15 °C higher desorption temperature than the H-BEA zeolite. However, higher loadings of La (6 and 9%) resulted in a decrease in HC storage/release, as was found in the HC TPD experiments. This is suggested to be caused by the steric hindrance induced by La. Shifts in the XRD measurements confirmed a large interaction between La and BEA. Zeolite SSZ-13 was unable to adsorb toluene due to the small pore size of the zeolite structure. In experiments with toluene, propene, and propane present at the same time in the storage step of HC TPD, it was found that propane desorbed from the ZSM-5 samples at a higher temperature and at higher concentrations (about four times higher) than propane alone (and H₂O). This indicates that interactions occurred between the different HC components that increased propane storage and, at the same time, increased the binding strength of propane. The in situ DRIFTS measurements confirmed that SSZ-13 did not trap toluene, as was found in the HC TPDs. In situ DRIFTS

data suggested that toluene was released faster for high La loading (6% La-BEA and 9% La-BEA) than for 2% La-BEA sample during the desorption process.

Author Contributions: Conceptualization, R.J., M.S., and L.O.; Data curation, R.J., P.H.H., and A.W.; Formal analysis, R.J., P.H.H., and A.W.; Methodology, R.J., M.S., and L.O.; Supervision, M.S. and L.O.; Writing—original draft, R.J.; Writing—review and editing, P.H.H., A.W., M.S. and L.O. All authors have read and agreed to the published version of the manuscript.

Funding: This research was funded by the Competence Centre for Catalysis, which is hosted by Chalmers University of Technology and financially supported by the Swedish Energy Agency, Chalmers and the member companies AB Volvo, ECAPS AB, Johnson Matthey AB, Preem AB, Scania CV AB and Umicore Denmark ApS.

Acknowledgments: This work has been performed within the Competence Centre for Catalysis, which is hosted by Chalmers University of Technology and financially supported by the Swedish Energy Agency, Chalmers and the member companies AB Volvo, ECAPS AB, Johnson Matthey AB, Preem AB, Scania CV AB and Umicore Denmark ApS.

Conflicts of Interest: The authors declare no conflict of interest.

Appendix A

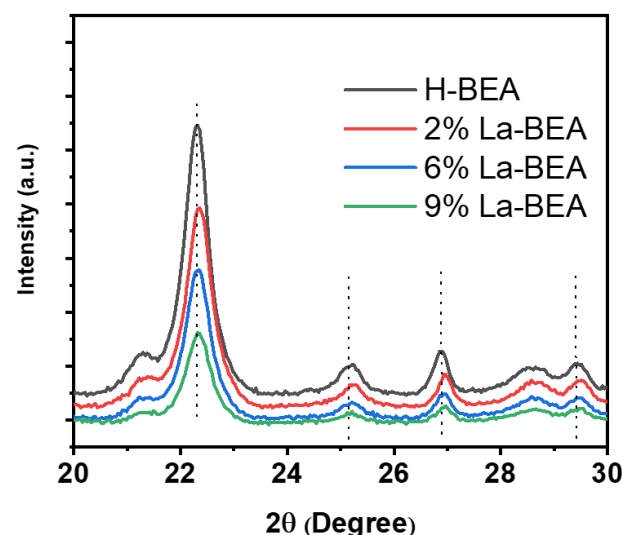


Figure A1. X-ray diffractograms of H-BEA and La-BEA with different loadings of La.

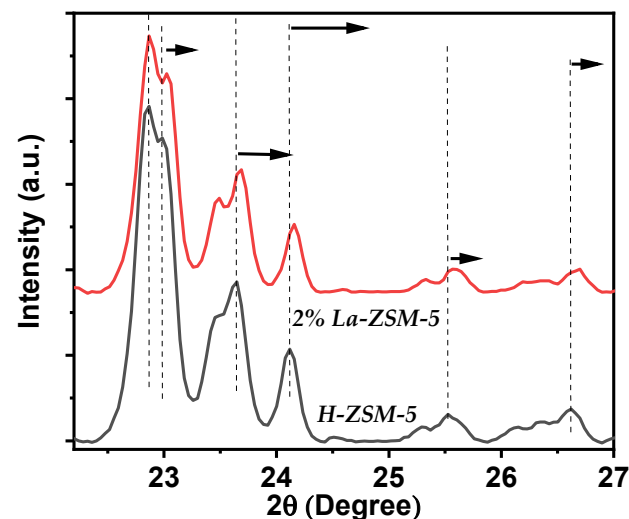


Figure A2. Enlargement of the X-ray diffractograms for H-ZSM-5 and 2% La-ZSM-5.

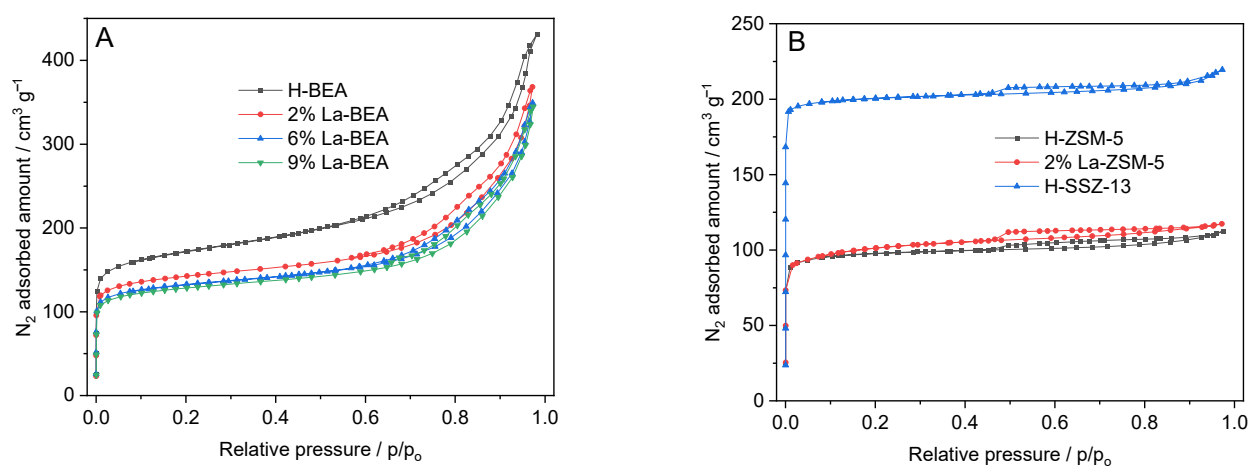


Figure A3. N_2 adsorption-desorption isotherms for (A) H-BEA and La-BEA with different La loading, and (B) H-SSZ-13, H-ZSM-5 and La-ZSM-5.

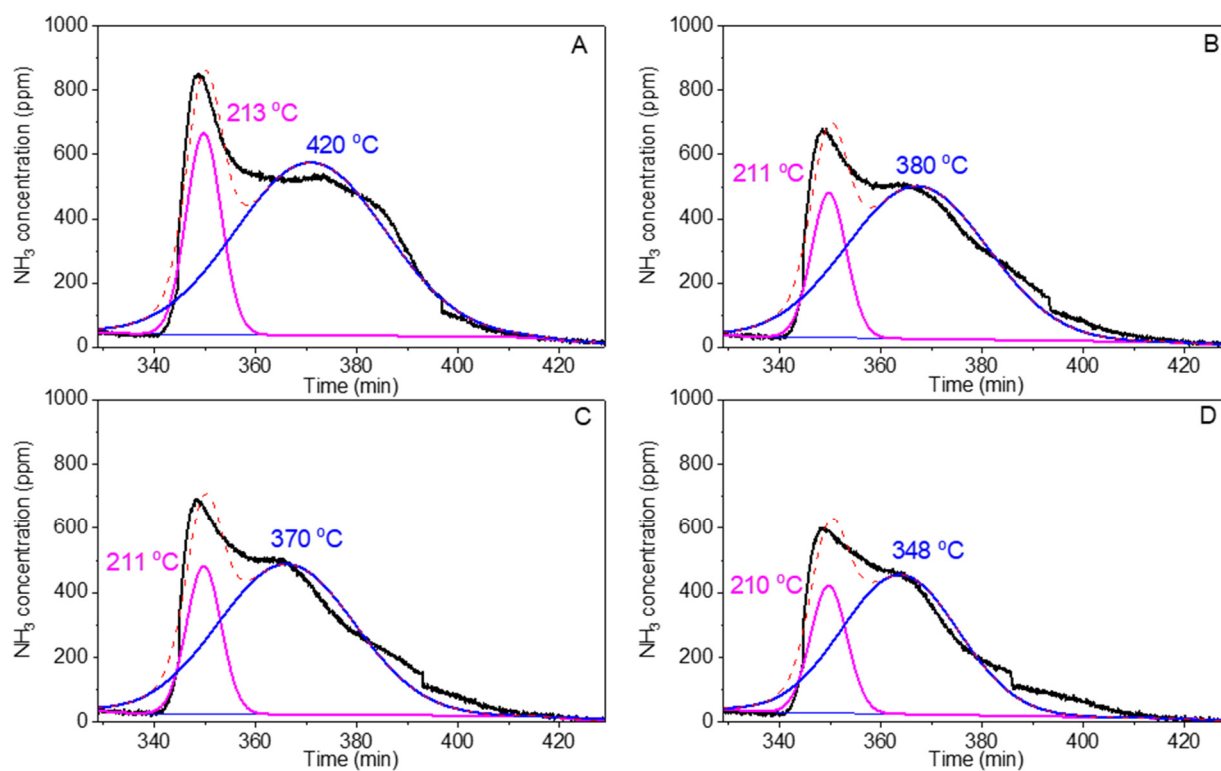


Figure A4. Deconvolution of the NH_3 -TPD profiles for (A) H-BEA, (B) 2% La-BEA, (C) 6%La-BEA and (D) 9% La-BEA.

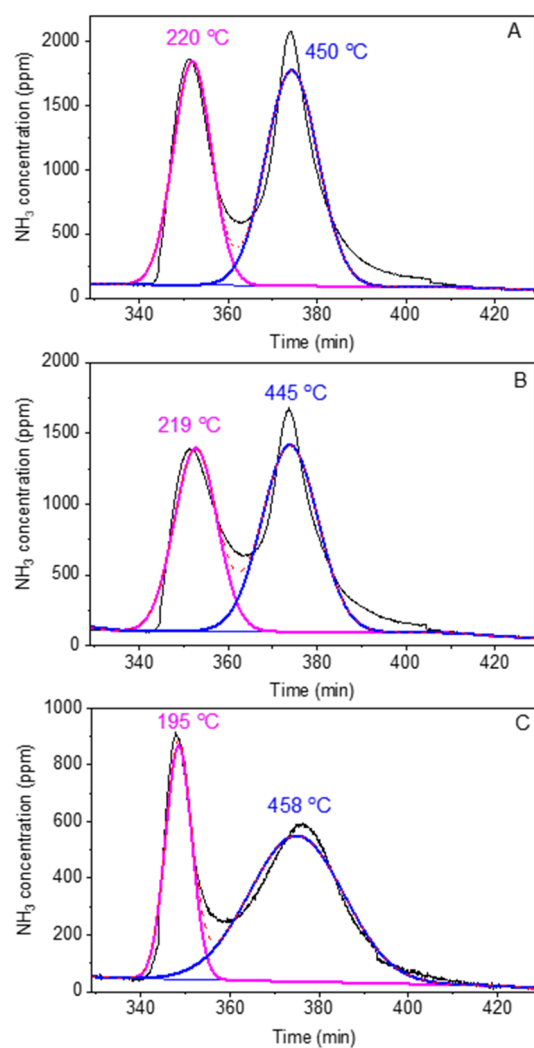


Figure A5. Deconvolution of the NH_3 -TPD profiles for (A) H-ZSM-5, (B) 2% La-ZSM-5 and (C) H-SSZ-13.

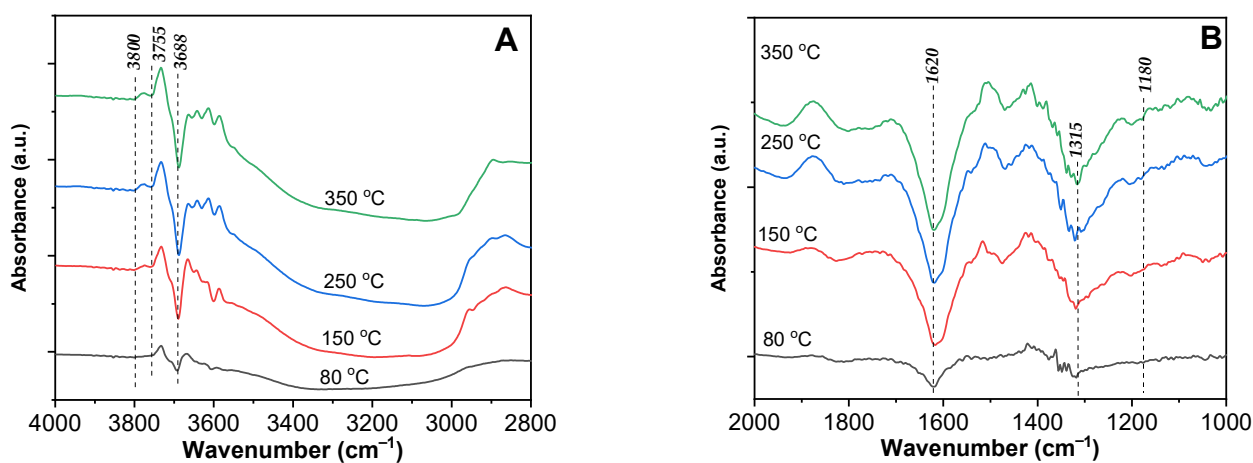


Figure A6. DRIFTS spectra during dry-toluene TPD experiments for H-SSZ-13: (A) High wave number and (B) low wave number. A stepwise measurement from 80–350 °C with only Ar present in the gas feed.

References

1. Park, J.-H.; Park, S.J.; Nam, I.-S.; Yeo, G.K.; Kil, J.K.; Youn, Y.K. A fast and quantitative assay for developing zeolite-type hydrocarbon trap catalyst. *Microporous Mesoporous Mater.* **2007**, *101*, 264–270. [\[CrossRef\]](#)
2. Kim, M.-Y.; Kyriakidou, E.A.; Choi, J.-S.; Toops, T.J.; Binder, A.J.; Thomas, C.; Parks, J.E.; Schwartz, V.; Chen, J.; Hensley, D.K. Enhancing low-temperature activity and durability of Pd-based diesel oxidation catalysts using ZrO₂ supports. *Appl. Catal. B Environ.* **2016**, *187*, 181–194. [\[CrossRef\]](#)
3. Du, S.; Tang, W.; Guo, Y.; Binder, A.; Kyriakidou, E.A.; Toops, T.J.; Wang, S.; Ren, Z.; Hoang, S.; Gao, P.-X. Understanding low temperature oxidation activity of nanoarray-based monolithic catalysts: From performance observation to structural and chemical insights. *Emiss. Control Sci. Technol.* **2017**, *3*, 18–36. [\[CrossRef\]](#)
4. Hazlett, M.J.; Epling, W.S. Spatially resolving CO and C₃H₆ oxidation reactions in a Pt/Al₂O₃ model oxidation catalyst. *Catal. Today* **2016**, *267*, 157–166. [\[CrossRef\]](#)
5. Lee, J.; Theis, J.R.; Kyriakidou, E.A. Vehicle emissions trapping materials: Successes, challenges, and the path forward. *Appl. Catal. B Environ.* **2019**, *243*, 397–414. [\[CrossRef\]](#)
6. Toops, T.J.; Binder, A.J.; Kunal, P.; Kyriakidou, E.A.; Choi, J.-S. Analysis of ion-exchanged ZSM-5, BEA, and SSZ-13 zeolite trapping materials under realistic exhaust conditions. *Catalysts* **2021**, *11*, 449. [\[CrossRef\]](#)
7. Han, D.; Jiaqiang, E.; Deng, Y.; Chen, J.; Leng, E.; Liao, G.; Zhao, X.; Feng, C.; Zhang, F. A review of studies using hydrocarbon adsorption material for reducing hydrocarbon emissions from cold start of gasoline engine. *Renew. Sustain. Energy Rev.* **2021**, *135*, 110079. [\[CrossRef\]](#)
8. Wesson, P.J.; Snurr, R.Q. Modified temperature programmed desorption evaluation of hydrocarbon trapping by CsMOR zeolite under cold start conditions. *Microporous Mesoporous Mater.* **2009**, *125*, 35–38. [\[CrossRef\]](#)
9. Yoshimoto, R.; Hara, K.; Okumura, K.; Katada, N.; Niwa, M. Analysis of toluene adsorption on Na-form zeolite with a temperature-programmed desorption method. *J. Phys. Chem. C* **2007**, *111*, 1474–1479. [\[CrossRef\]](#)
10. Kanazawa, T. Development of hydrocarbon adsorbents, oxygen storage materials for three-way catalysts and NO_x storage-reduction catalyst. *Catal. Today* **2004**, *96*, 171–177. [\[CrossRef\]](#)
11. Westermann, A.; Azambre, B.; Finqueneisel, G.; Costa, P.D.; Can, F. Evolution of unburnt hydrocarbons under “cold-start” conditions from adsorption/desorption to conversion: On the screening of zeolitic materials. *Appl. Catal. B Environ.* **2014**, *158–159*, 48–59. [\[CrossRef\]](#)
12. Moor, B.A.D.; Reyniers, M.-F.; Gobin, O.C.; Lercher, J.A.; Marin, G.B. Adsorption of C₂–C₈ n-alkanes in zeolites. *J. Phys. Chem. C* **2011**, *115*, 1204–1219. [\[CrossRef\]](#)
13. Rao, K.N.; Kim, M.-Y.; Song, J.; Na, S.; Han, H.S. *Cold-Start Hydrocarbon Speciation and Trap Materials for Gasoline Engines*; SAE Technical Paper, No. 2018-01-0940; SAE: Warrendale, PA, USA, 2018. [\[CrossRef\]](#)
14. Nakagawa, S.; Minowa, T.; Katogi, K.; Higashiyama, K.; Nagano, M.; Hamada, I. *A New Catalyzed Hydrocarbon Trap Control System for ULEV/SULEV Standard*; SAE Technical Paper, No. 2003-01-0567; SAE: Warrendale, PA, USA, 2003. [\[CrossRef\]](#)
15. Puértolas, B.; García-Andújar, L.; García, T.; Navarro, M.V.; Mitchell, S.; Pérez-Ramírez, J. Bifunctional Cu/H-ZSM-5 zeolite with hierarchical porosity for hydrocarbon abatement under cold-start conditions. *Appl. Catal. B Environ.* **2014**, *154–155*, 161–170. [\[CrossRef\]](#)
16. López, J.M.; Navarro, M.V.; García, T.; Murillo, R.; Mastral, A.M.; Varela-Gandía, F.J.; Lozano-Castelló, D.; Bueno-López, A.; Cazorla-Amorós, D. Screening of different zeolites and silicoaluminophosphates for the retention of propene under cold start conditions. *Microporous Mesoporous Mater.* **2010**, *130*, 239–247. [\[CrossRef\]](#)
17. Spoto, G.; Bordiga, S.; Ricchiardi, G.; Scarano, D.; Zecchina, A.; Borello, E. IR study of ethene and propene oligomerization on H-ZSM-5: Hydrogen-bonded precursor formation, initiation and propagation mechanisms and structure of the entrapped oligomers. *J. Chem. Soc. Faraday Trans.* **1994**, *90*, 2827–2835. [\[CrossRef\]](#)
18. Sarshar, Z.; Zahedi-Niaki, M.H.; Huang, Q.; Eić, M.; Kaliaguine, S. MTW zeolites for reducing cold-start emissions of automotive exhaust. *Appl. Catal. B Environ.* **2009**, *87*, 37–45. [\[CrossRef\]](#)
19. Azambre, B.; Westermann, A.; Finqueneisel, G.; Can, F.; Comparot, J.D. Adsorption and desorption of a model hydrocarbon mixture over HY zeolite under dry and wet conditions. *J. Phys. Chem. C* **2015**, *119*, 315–331. [\[CrossRef\]](#)
20. Westermann, A.; Azambre, B.; Chebbi, M.; Koch, A. Modification of Y faujasite zeolites for the trapping and elimination of a propene-toluene-decane mixture in the context of cold-start. *Microporous Mesoporous Mater.* **2016**, *230*, 76–88. [\[CrossRef\]](#)
21. Dorner, R.W.; Deifallah, M.; Catlow, C.R.A.; Corà, F.; Elangovan, S.P.; Okubo, T.; Sankar, G. Heteroatom-substituted microporous AFI and ATS structured materials for hydrocarbon trap: An insight into the aluminophosphate framework—Toluene interaction. *J. Phys. Chem. C* **2008**, *112*, 4187–4194. [\[CrossRef\]](#)
22. Daldoul, I.; Auger, S.; Picard, P.; Nohair, B.; Kaliaguine, S. Effect of temperature ramp on hydrocarbon desorption profiles from zeolite ZSM-12. *Can. J. Chem. Eng.* **2016**, *94*, 931–937. [\[CrossRef\]](#)
23. Park, J.-H.; Park, S.J.; Ahn, H.A.; Nam, I.-S.; Yeo, G.K.; Kil, J.K.; Youn, Y.K. Promising zeolite-type hydrocarbon trap catalyst by a knowledge-based combinatorial approach. *Microporous Mesoporous Mater.* **2009**, *117*, 178–184. [\[CrossRef\]](#)
24. Liu, X.; Lampert, J.K.; Arendarskii, D.A.; Farrauto, R.J. FT-IR spectroscopic studies of hydrocarbon trapping in Ag⁺-ZSM-5 for gasoline engines under cold-start conditions. *Appl. Catal. B Environ.* **2001**, *35*, 125–136. [\[CrossRef\]](#)
25. Ivanov, A.V.; Graham, G.W.; Shelef, M. Adsorption of hydrocarbons by ZSM-5 zeolites with different SiO₂/Al₂O₃ ratios: A combined FTIR and gravimetric study. *Appl. Catal. B Environ.* **1999**, *21*, 243–258. [\[CrossRef\]](#)

26. Burke, N.R.; Trimm, D.L.; Howe, R.F. The effect of silica:alumina ratio and hydrothermal ageing on the adsorption characteristics of BEA zeolites for cold start emission control. *Appl. Catal. B Environ.* **2003**, *46*, 97–104. [\[CrossRef\]](#)
27. Kang, S.B.; Kalamaras, C.; Balakotaiah, V.; Epling, W. Hydrocarbon trapping over Ag-beta zeolite for cold-start emission control. *Catal. Lett.* **2017**, *147*, 1355–1362. [\[CrossRef\]](#)
28. Kyriakidou, E.A.; Lee, J.; Choi, J.-S.; Lance, M.; Toops, T.J. A comparative study of silver- and palladium-exchanged zeolites in propylene and nitrogen oxide adsorption and desorption for cold-start applications. *Catal. Today* **2021**, *360*, 220–233. [\[CrossRef\]](#)
29. Takamitsu, Y.; Ariga, K.; Yoshida, S.; Ogawa, H.; Sano, T. Adsorption of toluene on alkali metal ion-exchanged ZSM-5 and β -zeolites under humid conditions. *Bull. Chem. Soc. Jpn.* **2012**, *85*, 869–876. [\[CrossRef\]](#)
30. Xu, L.; Lupescu, J.; Cavataio, G.; Guo, K.; Jen, H. The impacts of Pd in BEA zeolite on decreasing cold-start NMOG emission of an E85 fuel vehicle. *SAE Int. J. Fuels Lubr.* **2018**, *11*, 239–246. [\[CrossRef\]](#)
31. Lupescu, J.; Xu, L.; Jen, H.-W.; Harwell, A.; Nunan, J.; Alltizer, C.; Denison, G. A new catalyzed HC trap technology that enhances the conversion of gasoline fuel cold-start emissions. *SAE Int. J. Fuels Lubr.* **2018**, *11*, 411–442. [\[CrossRef\]](#)
32. Zelinsky, R.; Epling, W. Effects of multicomponent hydrocarbon feed on hydrocarbon adsorption–desorption and oxidation light-off behavior on a Pd/BEA hydrocarbon trap. *Catal. Lett.* **2019**, *149*, 3194–3202. [\[CrossRef\]](#)
33. Jonsson, R.; Woo, J.; Skoglundh, M.; Olsson, L. Zeolite beta doped with La, Fe, and Pd as a hydrocarbon trap. *Catalysts* **2020**, *10*, 173. [\[CrossRef\]](#)
34. Thommes, M.; Kaneko, K.; Neimark, A.V.; Olivier, J.P.; Rodriguez-Reinoso, F.; Rouquerol, J.; Sing, K.S.W. Physisorption of gases, with special reference to the evaluation of surface area and pore size distribution (IUPAC Technical Report). *Pure Appl. Chem.* **2015**, *87*, 1051–1069. [\[CrossRef\]](#)
35. Mintova, S.; Valtchev, V.; Onfroy, T.; Marichal, C.; Knözinger, H.; Bein, T. Variation of the Si/Al ratio in nanosized zeolite Beta crystals. *Microporous Mesoporous Mater.* **2006**, *90*, 237–245. [\[CrossRef\]](#)
36. Meng, F.; Wang, Y.; Wang, S. Methanol to gasoline over zeolite ZSM-5: Improved catalyst performance by treatment with HF. *RSC Adv.* **2016**, *6*, 58586–58593. [\[CrossRef\]](#)
37. Wang, D.; Jangjou, Y.; Liu, Y.; Sharma, M.K.; Luo, J.; Li, J.; Kamasamudram, K.; Epling, W.S. A comparison of hydrothermal aging effects on NH_3 -SCR of NO_x over Cu-SSZ-13 and Cu-SAPO-34 catalysts. *Appl. Catal. B Environ.* **2015**, *165*, 438–445. [\[CrossRef\]](#)
38. Zhang, L.; Qin, Y.; Zhang, X.; Gao, X.; Song, L. Further findings on the stabilization mechanism among modified Y zeolite with different rare earth ions. *Ind. Eng. Chem. Res.* **2019**, *58*, 14016–14025. [\[CrossRef\]](#)
39. He, D.; Zhao, Y.; Yang, S.; Mei, Y.; Yu, J.; Liu, J.; Chen, D.; He, S.; Luo, Y. Enhancement of catalytic performance and resistance to carbonaceous deposit of lanthanum (La) doped HZSM-5 catalysts for decomposition of methyl mercaptan. *Chem. Eng. J.* **2018**, *336*, 579–586. [\[CrossRef\]](#)
40. Deng, C.; Zhang, J.; Dong, L.; Huang, M.; Bin, L.; Jin, G.; Gao, J.; Zhang, F.; Fan, M.; Zhang, L.; et al. The effect of positioning cations on acidity and stability of the framework structure of Y zeolite. *Sci. Rep.* **2016**, *6*, 23382. [\[CrossRef\]](#)
41. Palomino, M.; Corma, A.; Jordá, J.L.; Rey, F.; Valencia, S. Zeolite rho: A highly selective adsorbent for CO_2/CH_4 separation induced by a structural phase modification. *Chem. Commun.* **2012**, *48*, 215–217. [\[CrossRef\]](#)
42. Sorenson, S.G.; Smyth, J.R.; Noble, R.D.; Falconer, J.L. Correlation of crystal lattice expansion and membrane properties for MFI zeolites. *Ind. Eng. Chem. Res.* **2009**, *48*, 10021–10024. [\[CrossRef\]](#)
43. Gor, G.Y.; Huber, P.; Bernstein, N. Adsorption-induced deformation of nanoporous materials—A review. *Appl. Phys. Rev.* **2017**, *4*, 011303. [\[CrossRef\]](#)
44. Al-Dughaiter, A.S.; Lasa, H.D. HZSM-5 zeolites with different $\text{SiO}_2/\text{Al}_2\text{O}_3$ ratios. Characterization and NH_3 desorption kinetics. *Ind. Eng. Chem. Res.* **2014**, *53*, 15303–15316. [\[CrossRef\]](#)
45. Bok, T.O.; Andriako, E.P.; Knyazeva, E.E.; Ivanova, I.I. Engineering of zeolite BEA crystal size and morphology via seed-directed steam assisted conversion. *RSC Adv.* **2020**, *10*, 38505–38514. [\[CrossRef\]](#)
46. Engtrakul, C.; Mukarakate, C.; Starace, A.K.; Magrini, K.A.; Rogers, A.K.; Yung, M.M. Effect of ZSM-5 acidity on aromatic product selectivity during upgrading of pine pyrolysis vapors. *Catal. Today* **2016**, *269*, 175–181. [\[CrossRef\]](#)
47. Li, Z.; Navarro, M.T.; Martínez-Triguero, J.; Yu, J.; Corma, A. Synthesis of nano-SSZ-13 and its application in the reaction of methanol to olefins. *Catal. Sci. Technol.* **2016**, *6*, 5856–5863. [\[CrossRef\]](#)
48. Serra, R.M.; Miró, E.E.; Bolcatto, P.; Boix, A.V. Experimental and theoretical studies about the adsorption of toluene on ZSM5 and mordenite zeolites modified with Cs. *Microporous Mesoporous Mater.* **2012**, *147*, 17–29. [\[CrossRef\]](#)
49. Yue, Y.; Fu, J.; Wang, C.; Yuan, P.; Bao, X.; Xie, Z.; Basset, J.-M.; Zhu, H. Propane dehydrogenation catalyzed by single Lewis acid site in Sn-Beta zeolite. *J. Catal.* **2021**, *395*, 155–167. [\[CrossRef\]](#)
50. Sharma, M.; Shane, M. Hydrocarbon-water adsorption and simulation of catalyzed hydrocarbon traps. *Catal. Today* **2016**, *267*, 82–92. [\[CrossRef\]](#)
51. Czaplewski, K.F.; Reitz, T.L.; Kim, Y.J.; Snurr, R.Q. One-dimensional zeolites as hydrocarbon traps. *Microporous Mesoporous Mater.* **2002**, *56*, 55–64. [\[CrossRef\]](#)
52. Li, X.; Zhu, Z.; Zhao, Q.; Wang, L. Photocatalytic degradation of gaseous toluene over ZnAl_2O_4 prepared by different methods: A comparative study. *J. Hazard. Mater.* **2011**, *186*, 2089–2096. [\[CrossRef\]](#)
53. Sanati, M.; Andersson, A. DRIFT study of the oxidation and the ammoxidation of toluene over a $\text{TiO}_2(\text{B})$ -supported vanadia catalyst. *J. Mol. Catal.* **1993**, *81*, 51–62. [\[CrossRef\]](#)
54. Nagao, M.; Suda, Y. Adsorption of benzene, toluene, and chlorobenzene on titanium dioxide. *Langmuir* **1989**, *5*, 42–47. [\[CrossRef\]](#)

-
55. Trombetta, M.; Busca, G.; Storaro, L.; Lenarda, M.; Casagrande, M.; Zambon, A. Surface acidity modifications induced by thermal treatments and acid leaching on microcrystalline H-BEA zeolite. A FTIR, XRD and MAS-NMR study. *Phys. Chem. Chem. Phys.* **2000**, *2*, 3529–3537. [[CrossRef](#)]
 56. Marques, J.P.; Gener, I.; Ayrault, P.; Bordado, J.C.; Lopes, J.M.; Ribeiro, F.R.; Guisnet, M. Dealumination of HBEA zeolite by steaming and acid leaching: Distribution of the various aluminic species and identification of the hydroxyl groups. *Comptes Rendus Chim.* **2005**, *8*, 399–410. [[CrossRef](#)]
 57. Su, B.-L.; Norberg, V. Characterization of the Brønsted acid properties of H(Na)-Beta zeolite by infrared spectroscopy and thermal analysis. *Zeolites* **1997**, *19*, 65–74. [[CrossRef](#)]
 58. Yang, C.; Xuaf, Q. States of aluminum in zeolite β and influence of acidic or basic medium. *Zeolites* **1997**, *19*, 404–410. [[CrossRef](#)]
 59. Du, J.; Qu, Z.; Dong, C.; Song, L.; Qin, Y.; Huang, N. Low-temperature abatement of toluene over Mn-Ce oxides catalysts synthesized by a modified hydrothermal approach. *Appl. Surf. Sci.* **2018**, *433*, 1025–1035. [[CrossRef](#)]
 60. Wang, M.; Zhang, F.; Zhu, X.; Qi, Z.; Hong, B.; Ding, J.; Bao, J.; Sun, S.; Gao, C. DRIFTS evidence for facet-dependent adsorption of gaseous toluene on TiO₂ with relative photocatalytic properties. *Langmuir* **2015**, *31*, 1730–1736. [[CrossRef](#)]
 61. Olsson, L.; Wijayanti, K.; Leistner, K.; Kumar, A.; Joshi, S.Y.; Kamasamudram, K.; Currier, N.W.; Yezerets, A. A multi-site kinetic model for NH₃-SCR over Cu/SSZ-13. *Appl. Catal. B Environ.* **2015**, *174–175*, 212–224. [[CrossRef](#)]